TURBULENT SHEAR LAYERS AND WAKES

Garry L. Brown[1] and Anatol Roshko[2]

1. Introduction

The subject for this session, turbulent shear layers and wakes, can be considered as a subset of free turbulent shear flows. It was covered in Marseille in 1961 in a session that had only two lectures, one by Liepmann and the other by Coles. Liepmann, in his summary, refers to the discovery by flow visualization of a sharp interface separating the multi-scale, vorticity field of the 'turbulent' flow from the outer, irrotational, flow (Figure 1), as the 'single most important experimental finding in turbulent shear flows'. It was observed by Corrsin (1943) and its features were further recognized by Townsend (1949). Corrsin and Kistler (1954), especially, considered the properties of this interface to be important for the entrainment of irrotational fluid into the turbulent region.

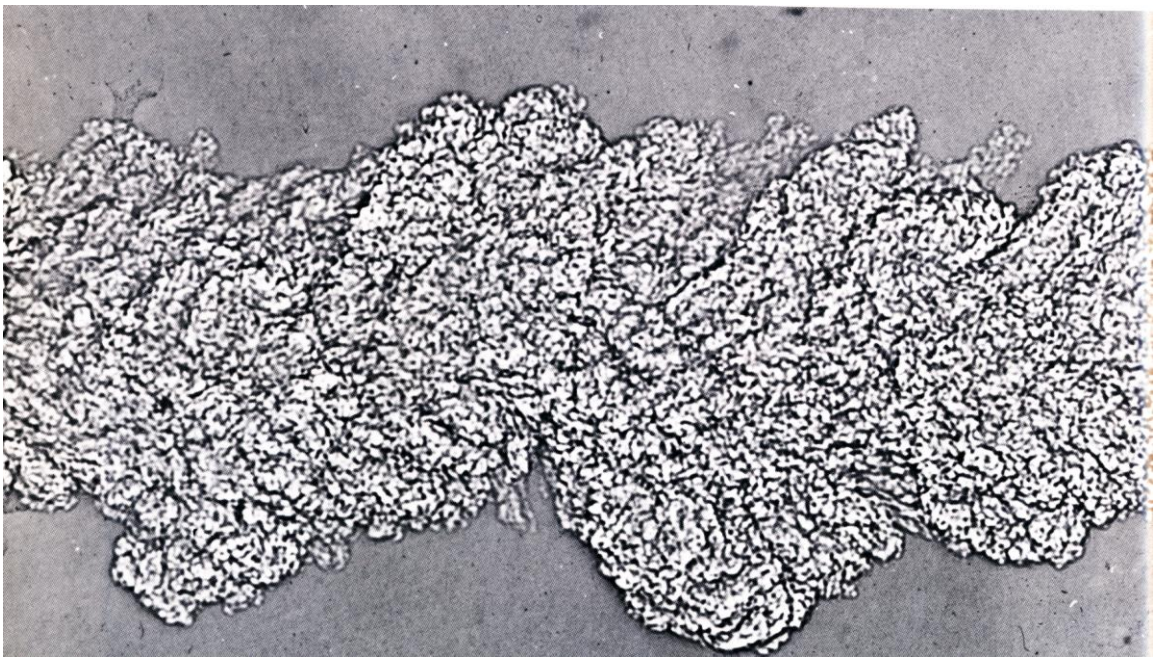

Figure 1 The wake of a bullet (BRL Aberdeen Proving Ground 1954)

[1] Princeton University
[2] California Institute of Technology

Liepmann described the fluid that has small scale rotational motions and in which the large scale motion develops, as a 'turbular fluid', whereas earlier Townsend (1956) had made the same identification but he called it the 'turbulent fluid', apparently assigning to it the principal role in the development of the mean flow. He postulated a 'typical' large scale eddy and sought to understand how the mean strain field in free shear flows interacted with large eddies within the 'turbulent' (i.e. 'turbular') fluid to provide energy to these large eddies. This large scale motion was postulated to be associated with an eddy which was oriented not in the span-wise direction (the direction of the mean vorticity in plane flow) but in a plane normal to the span-wise direction. He had put forward an energy equilibrium hypothesis for the relationship between the large eddies and the "main turbulence".

By 1976 however, in the preface to his second edition, Townsend commented that 'Although my current views have been developed from those I held in 1956 they have undergone considerable change. Perhaps I should thank especially Dr H.L. Grant who, as my research student, began the process by demolishing a complete chapter before the ink was wholly dry'. He was referring to his Chapter 6 in the 1956 edition 'Free Turbulence; Motion of the Large Eddies'.
Correlation measurements within a turbulent wake by Grant (1958) had resulted in a depiction of a **mean** large-eddy structure in the far wake (x/D=533), shown in Figure 2a. Subsequently, Payne and Lumley (1967) applied Proper Orthogonal Decomposition to the measurements of Grant and arrived at the structure shown in Figure 2b.

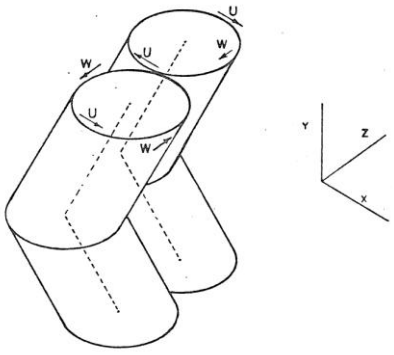

Figure 3. Schematic model of the vortex pair eddy.

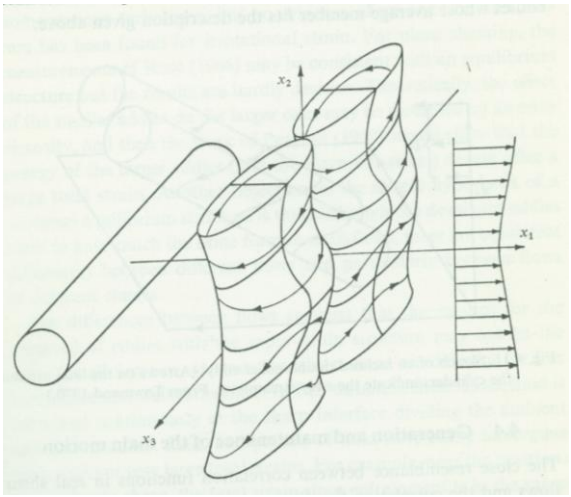

Figure 2a (Grant 1958)

Figure 2b (Payne and Lumley 1967)

There was no discussion of these early measurements of structure at the 1961 Colloquium. An **instantaneous** structure with its vorticity in the *y* direction and across the whole wake has not been observed directly. With various advances in experimental methods and the advent of modern signal processing, however, there have been measurements made (e.g. Antonia, Browne, Bisset and Fulachier (1987)) to help understand what **instantaneous** large structures could account for the **mean** structure

which emerged from these early measurements as a double roller (Figures 2a and 2b) with axes **normal** to the plane of the wake.

Later, Townsend (1976) explored another idea in which the turbular fluid was considered to behave like a **viscoelastic fluid**. Further investigations of the effects of strain on homogeneous turbulence were made by Lumley in his paper 'Toward a turbulent constitutive relation' (Lumley 1970).

Liepmann's view of the relation of turbular fluid to large structure had been influenced by a then-recent observation (Roshko 1961) of well organized vortex shedding in the near wake of a circular cylinder at a Reynolds number of 10^7. This indicated a similarity between the vortex-shedding instability at much lower values of Re (of order 100) in viscous fluid and the one at high Re, presumably in turbular fluid. It also suggested that the large structure far downstream in a turbulent wake might be related to large-scale instability of the turbular fluid within the boundaries of the wake. In his lecture he discussed at some length a numerical simulation of a **temporal** wake (Figure 3) by Abernathy and Kronauer (subsequently published in 1962) in which two parallel vortex sheets, modeled by point vortices and separated by a 'thickness' δ, represent the initial wake.

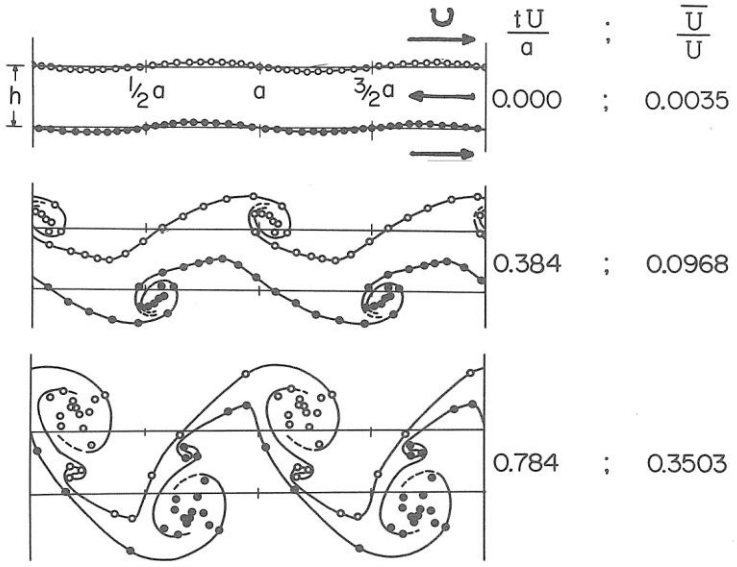

Figure 3 Abernathy and Kronauer (1962)

The unstable response to a perturbation of scale $\lambda > \delta$ leads to both large and small structure. Liepmann noted particularly that in addition to the expected large organized structure related to λ there were also small vortical structures: 'Remembering that two-dimensional vortex motion is so much simpler than general vortex motion, one gets here a fascinating glimpse into the rapid randomization by vortex interactions and a demonstration of the statistical character of turbulence *proper*' (our italics).

In the following paper, 'Interfaces and Intermittency in Turbulent Shear Flows', Coles included jets and wakes (Figure 1) as well as examples from wall-bounded flows, namely 'turbulent spots' in boundary layers, 'slugs' in pipe flow and spiral bands in circular Couette flow, which occur in **transition** regions of **wall-bounded** flows. The interface phenomenon on which Liepmann concentrated occurs in fully developed, **free** turbulent flows, as in Figure 1.

In his closing Comments on Free Turbulence, Liepmann reiterated the experimental observation that 'free turbulent flows consist of regions of nearly homogeneous turbulence and irrotational regions. The dividing boundary is sharp and its location a stochastic function of time with scales one order of magnitude larger than the scales of the homogeneous turbulence.' Problems requiring further attention included the following items (abstracted from his longer statements):

(a) The effect of strain on homogeneous turbulence
. (b) The structure of turbulent interfaces
(c) The instability of turbulent flow.
(d) The heuristic model of non-Newtonian fluid….to describe the *instabilities and transport* properties in free turbulent flows. (Our italics)

The suggestion in item (d) that a 'turbular' fluid might be represented by some kind of local constitutive relationship reflected a more general theme in which the action of turbulence in diffusing the momentum had been sought through an eddy viscosity and local mean strain, for example by Prandtl (1925) and Taylor (1915). The concept of homogeneous isotropic turbulence introduced by Taylor (1935) provided a conceptual basis, as in Townsend (Section 6.3, 1956), for a 'turbular' fluid. It also marked something of a divide in research interests. Local dispersion and the response of homogeneous turbulence to a pure strain, for example, were pursued on one path while well-defined free turbulent shear flows, where dimensional analysis and similarity arguments for the mean equations of motion are powerful tools, were pursued experimentally on the other. The latter led to a number of 'canonical' free turbulent shear flows (self-preserving or equilibrium flows which no longer depend on their initial development) in which there is only one local velocity scale, one local length scale and some global constraint (for example the drag for wakes or the thrust for jets). Empirical constants in such 'canonical' free shear flows essentially guided the development of practical, local, constitutive relationships in turbulence models but the 1961 Colloquium did not have any discussion of modeling for applications nor does the present one. The reason is partly because this 'local' concept is well-known to be an important practical tool but a misleading representation of the mechanics, especially for free turbulent shear flows. The mechanics by which the self-similar state at one scale becomes self-similar at a larger scale, for example, is hidden in the empirical constants.

It was approximately a decade after the 1961 Colloquium that the picture that would have been drawn at the time of the Marseille meeting for the free shear layer (mixing layer), radically changed. The shadowgraph pictures and movies that we and others obtained (Brown and Roshko (1974)), revealed the essential role of the large-scale, predominantly

two-dimensional span-wise vorticity and the essential role of the Biot-Savart interaction in the 'amalgamation' or 'clumping' of this vorticity to larger and larger scales. Figure 4(a) is a sequence from our movie between gas mixtures of the same density but different refractive index (one monatomic the other diatomic) and Figure 4(b) a simultaneous plan view and side view.

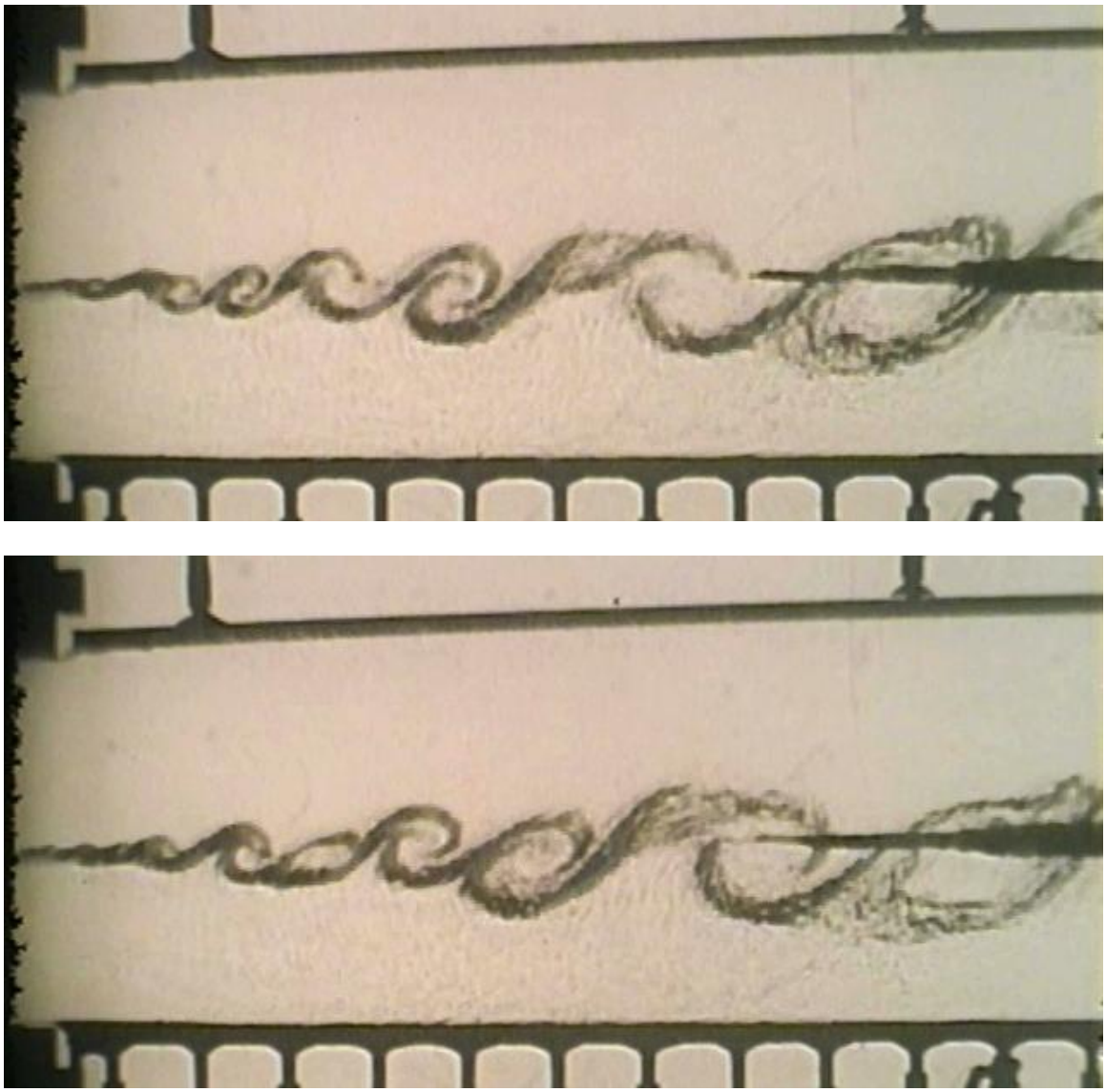

Figure 4(a), Mixing layer, Constant density, 8 atm U2/U1=0.38 Sequence of three shadowgraphs from a high speed movie separated by a fixed time interval. (the same experimental set-up was used for the results in Figure 5)

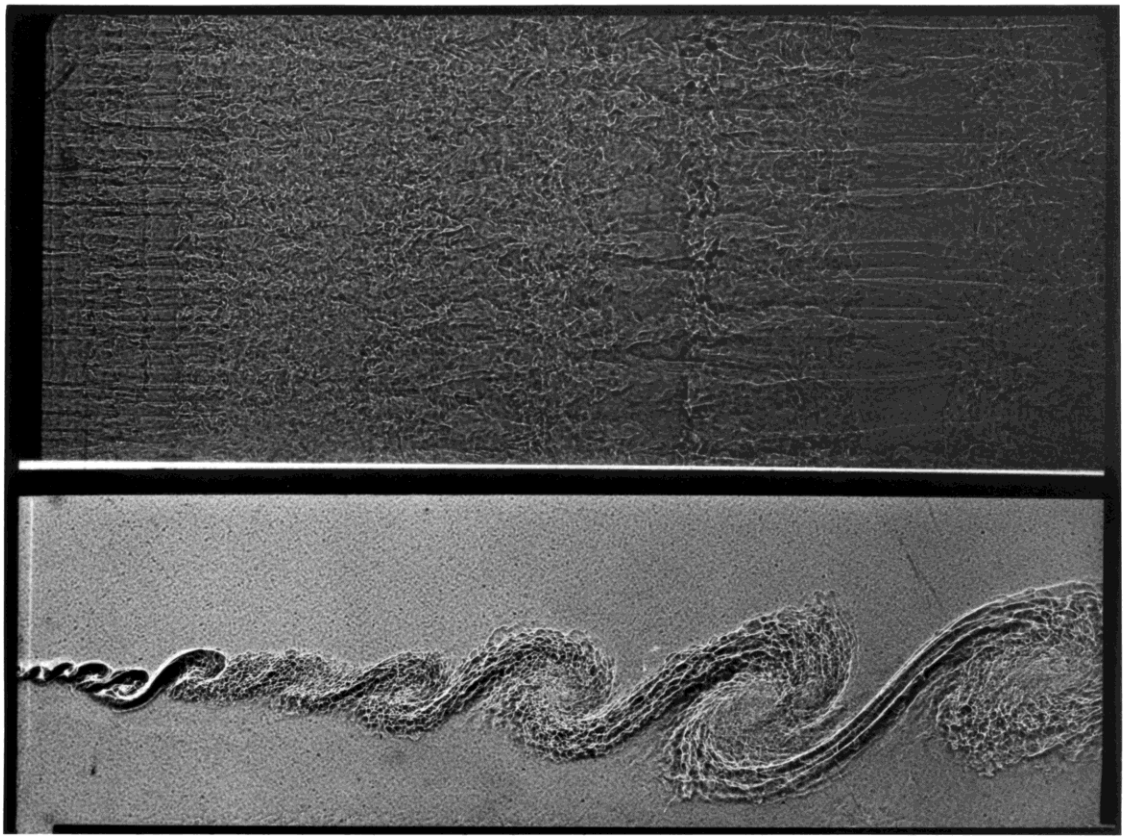

Figure 4(b), Mixing layer, Constant density, 4 atm U2/U1=0.38. Side and Plan view (Konrad)

This picture of 'coherent structure' and the implied mechanics in a high Reynolds number turbulent shear flow was quite different from Townsend's (1956) large eddy hypothesis. The latter was influenced by tentative energy considerations which are not invoked at all, for example, in a two-dimensional Biot-Savart interpretation of the large structure. Similarly from Figure 4(b) the three-dimensionality in the flow appears 'to ride on' and be reinforced by the two dimensional large-scale vortical structure and any supposed constitutive relationship for this small scale motion is at best weakly connected to the primary Biot-Savart mechanics of the large scale motion. The plan view shows the effect of the primary strain (especially in the 'braids' between the large scale vortical motion) in amplifying stream-wise vorticity but it is evidently important to the production of small scales rather than to the large scales which control the growth rate and shear stress.

At approximately the same time the near wall structure in the turbulent boundary layer, revealed in the hydrogen bubble flow visualization of Kline et al. (1967), provided a major departure from previous understandings.

That it was a major change, 'which caught the imagination of fluid dynamicists', (Narasimha, Whither Turbulence? Meeting (1989) P.37) is evident from the premise and proceedings of that meeting. In the Session on 'The role of Coherent Structures', Cantwell (P. 97) drew attention to insights that this structure provided and in particular the future possibilities for simulation, new opportunities for developing explanations of underlying physical mechanisms and for control.

From this point of view what has seemed increasingly necessary is to connect a 'structure' view to the underlying mechanics, which is best revealed for the rotational motion of turbulence through the vorticity equation with the necessary connection to the velocity field (viscous or inviscid flow) through the Biot-Savart relationship. Notwithstanding Taylor's vorticity transport theory {in 2D (1915, Vol. 2 paper 1) and in 3D (1932, Vol. 2 paper 24)} and Kuechemann's subsequent view (1965) that 'vortices are the muscle and sinews of fluid motion' there was mainly passing mention of vorticity in the papers presented and in the recorded discussion of the 1961 Colloquium.

That a vorticity view has not had more experimental emphasis, despite the more recent focus on 'coherent structure', is because of the difficulty in measuring the vorticity. For computations of the Navier stokes equations, however, there is no such constraint. It is this view that seems particularly appropriate for this meeting and we shall emphasize it in the context of free shear layers and wakes.

One of the immediate consequences of the results shown in Figure 4(a) and 4(b) was an expectation that, for this case, a two-dimensional flow driven by a Biot-Savart interaction between 'clumps' of vorticity of the same sign, may account for the principal mechanics. Attempts were made to simulate this mechanics using an initial distribution of point vortices to simulate a small perturbation to a vortex sheet of some initial thickness (Ashurst 1979, Aref 1980, for example). The growth rates were determined from mean velocity profiles as was the Reynolds stress profile but the direct connection with the vorticity flux (as in section 2 below) was not made. Recently, results from much more extensive calculations for both the temporal and spatial case, using this two-dimensional 'vortex gas' approach (Narasimha and Suryanarayanan (2011)), have been obtained (section 3 below). Similarly a computational study of a spatial, two-dimensional (high Reynolds number but viscous) mixing layer has been completed (section 3). Some comparisons with the 3D experimental results are mentioned below along with the experimental observations on the development of three dimensionality and its central contribution to 'mixing' and weak contribution to Reynolds stress.

2. Reynolds stress and the Vorticity flux

It is the **gradient** in Reynolds stress which enters the mean momentum equation and for incompressible flow this gradient is directly connected with the vorticity flux (as given in

more detail in Appendix I). In particular, for plane turbulent shear flow the familiar gradient in Reynolds stress is

$$\frac{\partial(-\overline{u'v'})}{\partial y} = \overline{\omega_z' v'} - \overline{\omega_y' w'} - \frac{\partial}{\partial x}(\frac{1}{2}\overline{q'^2}), \tag{2.1}$$

Replacing the gradients of Reynolds stress by these vorticity-velocity correlations was a starting point for Taylor's vorticity transport theory.
For temporal turbulent shear layers (and Channel flow or Couette flow) the x derivative is identically zero and it is typically a higher order term for spatially growing shear flows (within the 'boundary layer' approximation). In this case the Reynolds stress gradient is obtained directly from the flux of vorticity.

(Note, in passing, that for strictly two-dimensional models of a temporal rotational flow (such as a 2D instability) the Reynolds stress gradient is obtained directly from $\overline{\omega_z' v'}$ (sometimes interpreted as a 'vortex force'), i.e the only contribution is from the rotational fluid. The spatially averaged Reynolds stress in the flow, which accounts for the rate of change of momentum on a particular plane, is obtained from the integration of $\overline{\omega_z' v'}$ from infinity. If, instead, this Reynolds stress were obtained directly from the spatial average of $\overline{u'v'}$ there may be a substantial contribution from the irrotational fluid if on any plane there are local regions of rotational and irrotational fluid! This is a subtlety not always appreciated.)

The vorticity equation, which follows from the Navier Stokes equations, is

$$\frac{\partial \boldsymbol{\omega}}{\partial t} + \boldsymbol{u}\cdot\nabla\boldsymbol{\omega} = \boldsymbol{\omega}\cdot\nabla\boldsymbol{u} + \nu\nabla^2\boldsymbol{\omega}\ , \tag{2.2}$$

and the Biot-Savart relationship determines the velocity field that is necessarily associated with the vorticity field.

$$\boldsymbol{u}_\omega(x,y,z) = \iiint \frac{\boldsymbol{\omega}(\xi,\eta,\zeta)\times\boldsymbol{s}}{4\pi s^3} d\xi d\eta d\zeta\ . \tag{2.3}$$

In terms of the vorticity, the corresponding velocity field is evidently a **global** quantity found by integrating over the whole vorticity field, so that a velocity-vorticity correlation cannot be thought of as determined solely from the local velocity or vorticity.

An alternative form of equation (2.2) written in conservation form is

$$\frac{\partial \omega_i}{\partial t} + \frac{\partial}{\partial x_k}(u_k\omega_i - \omega_k u_i - \nu\frac{\partial \omega_i}{\partial x_k}) = 0 \tag{2.4}$$

and when integrated over a volume fixed in space it gives (Gauss' theorem)

$$\frac{d}{dt}\iiint \omega_i dV + \iint (u_k\omega_i - \omega_k u_i - \nu\frac{\partial \omega_i}{\partial x_k})n_k dS = 0 \ . \qquad (2.5)$$

For a turbulent flow which is <u>steady</u> in a time mean sense this equation is

$$\iint (U_k\Omega_i - \Omega_k U_i + \overline{u_k'\omega_i'} - \overline{\omega_k' u'}_i - \nu\frac{\partial \Omega_i}{\partial x_k})n_k dS = 0\,. \qquad (2.6)$$

For a two-dimensional flow around a symmetrical body, (e.g. a circular cylinder) the mechanics is illuminated by this equation. If the fixed volume (control volume) includes the upper surface of the body and the upper half plane it is clear from equation (2.6) that the source of span-wise vorticity is on that part of the boundary which is a solid surface (e.g. the cylinder surface). Downstream there is a flux out of the volume on a plane perpendicular to the flow at $x = X$ which is less than that which is supplied upstream from the surface of the body and that is entirely because of the net flux of vorticity out of the volume across the plane $y = 0$, namely

$$\int_{-D/2}^{X}\left[-\left(\overline{v'\omega_z'} - \overline{\omega_y' w'}\right) + \nu\frac{\partial \Omega}{\partial y}\right]dx\,. \qquad (2.7)$$

(since, by symmetry, $V = 0$ on this plane).

The mechanics by which the mean vorticity is 'lost' ('cancelled') across $y = 0$ in the near wake is not well known but it is accessible today through DNS and LES calculations. Within approximately one diameter from the base of the cylinder, the flux of vorticity across the normal plane is less than one half of that supplied from the surface of the body (a fact that was known to early experimenters from direct measurements of mean velocity profiles). Similarly in the far wake a question which arises is - To what extent does a 'large scale' motion, which is dependent for example on the 'clumping' of vorticity to larger scales due to a two-dimensional and/or three-dimensional instability, contribute to the all important turbulent flux $\left(\overline{v'\omega_z'} - \overline{\omega_y' w'}\right)$. These are points to which we return in section 4 below.

3. Some further results, conclusions and questions on the free shear layer

- **Coherent structure and Biot-Savart considerations**

The quasi 'two-dimensional structure' observed in the photographs was in direct conflict with the anticipated structure (e.g. the Townsend model) and many attempts were made to examine its robustness to perturbation and its persistence to even higher Reynolds numbers etc. Figure 7(b) (Breidenthal), for example, shows the result of very substantial

three-dimensional perturbations at the splitter plate and the recovery, not far downstream, of the dominant span-wise structure.

The global constraints on the asymptotic mixing layer require linear growth and allow self-similarity, which is demonstrated by the mean velocity profile measurements shown in Figure 5. It follows that the growth of the coherent structures cannot proceed continuously and that their merging must occur randomly. Such large scale interactions will contribute to the low wave number components of the energy spectrum.

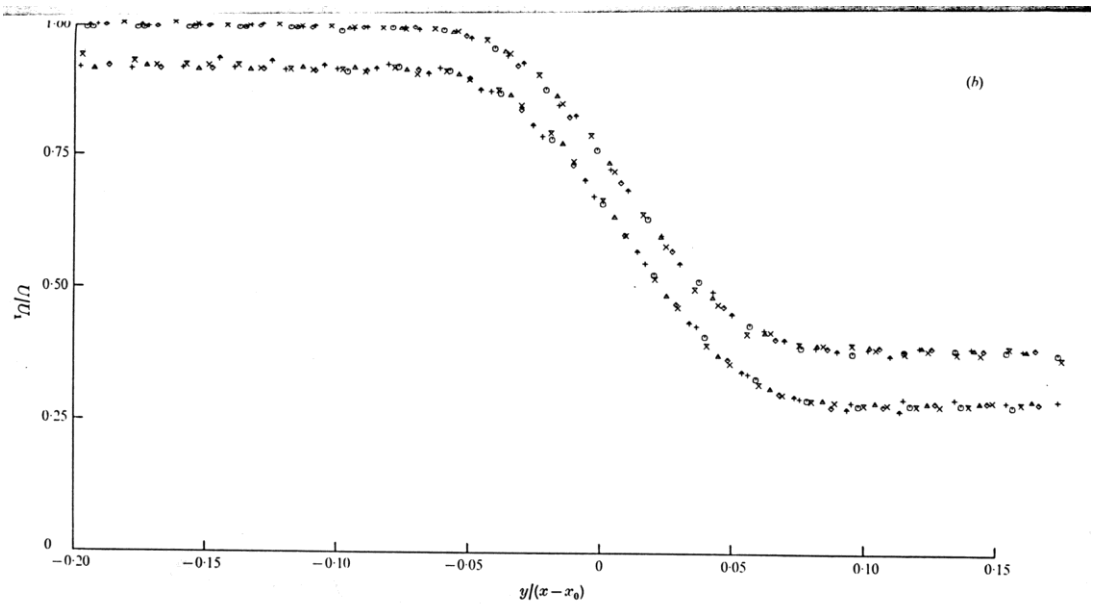

FIGURE 9. Velocity profiles of mixing layers in air, obtained from simultaneous traverse of Pitot tube and hot-wire probe. (Hot-wire profile is displaced downward for clarity.) (*a*) $U_1 = 1000\,\mathrm{cm\,s^{-1}}$, $U_2 = 143\,\mathrm{cm\,s^{-1}}$, pressure = 7 atm. $x_0 = -0{\cdot}25$ in. (*b*) $U_1 = 1000\,\mathrm{cm\,s^{-1}}$, $U_2 = 382\,\mathrm{cm\,s^{-1}}$, pressure = 7 atm. $x_0 = -0{\cdot}38$ in. x(in.): ⊙, △, 0·5; ×, 0·75; ↑, ⊠, 1·00; +, 1·50; ◇, 2·00; Z, 2·50; Y, 3·00; ⊠, 3·50.

Figure 5. Similarity in the mean velocity profile for $U_2/U_1 = 0.382$ obtained from redundant hotwire and Pitot-static measurements at seven streamwise locations, as noted in part (b) of the caption.

The Reynolds number, $(U_1 - U_2)\delta_\omega / \nu$, of the mixing layer at the stations measured in Figure 5(a) increases by a factor of five from 0.6 to $2.9x10^4$, suggesting that the growth rate is independent of Reynolds number. In terms of the vorticity thickness, $\delta_\omega = (U_1 - U_2)/(\partial U/\partial y)_{\max}$, this growth rate is $d\delta_\omega / dx = \delta'_\omega = 0.088$. This is close to the value, 0.088, obtained by Narasimha and Suryanarayanan (2011) in a (so-far unpublished) **two-dimensional** numerical simulation at the same value of U_2 / U_1. The 'vortex gas' method used in the simulation implies independence of viscosity. The comparison is striking, particularly in the close agreement with the 'real' three-dimensional flow, which is shown in Figure 4(b). In a two-dimensional Navier-Stokes simulation by Carton de Wiart and Winckelmans (2011), also not yet published, of a mixing layer at $U_2/U_1 = 0.38$, values of the growth rate varied from 0.082 to 0.087 with Reynolds number from $0.7 - 2.5\times10^5$. It is clear that there remains some uncertainty in

establishing a definitive value for the growth rates in two-dimensional and three-dimensional shear layers.
Nevertheless these comparisons between the two-dimensional calculations and the three-dimensional data lend support to the hypothesis that the Biot-Savart interaction between 'clumps' of vorticity (whose span-wise component is in the same direction) over scales of the order of the thickness of the layer, plays a dominant role in determining the Reynolds stress; the more local contributions from three-dimensional motions are much less important.

- **Entrainment, Mixing and the 'mixing transition'**

At the time of the Marseille meeting a plane boundary between the 'turbular' fluid and the potential flow was considered an 'active' boundary. Townsend, for example, notes (Section 3.9) that the 'boundary region between a semi-infinite field of homogeneous turbulence and the adjacent undisturbed fluid' (our emphasis) is 'the simple entrainment by turbulent fluid of adjacent non-turbulent fluid, which is the basic process in the spread of wakes, jets ---'. This hypothesis was found not to be the basic mechanism for the mixing layer. Figure 4(a) suggests instead that an important mechanism that leads to the regions of 'engulfed' but unmixed fluid comes from the velocity field of the irrotational fluid, which is induced by the 'large scale' span-wise vorticity. The irrotational fluid is 'engulfed' as the coherent structures evolve and merge to form larger structures and the three-dimensional 'small-scale' mixing occurs without a strong influence on the larger scale motion. Thus, in a purely two-dimensional temporal shear layer, fluid from both free streams would be found in the regions between the layers of vorticity which form the 'coherent structures' of such a flow. If in addition to the large scale motion there is a smaller scale three-dimensional motion this 'engulfed' fluid would be mixed more uniformly. Correspondingly, in the 3D case there need be no change in the mean Reynolds stress but a considerable increase in the area of the interface between the two separate fluids.
Probing measurements in gases by Konrad (1977) and later the direct measurements of reactant product in water by Breidenthal (1978, 1981), (Figure 6) identified a 'mixing transition' Reynolds number for the mixing layer ($\frac{\Delta U \delta_\omega}{\nu} \approx 2-8\times10^3$) over which there is a substantial increase in small scale 'mixing' and, more precisely, 'mixing' at diffusive scales. Photographs by Bernal (1981) showed the role of small scale streamwise vorticity in this mixing and the reinforcement of this vorticity by the straining motion between large structures (also evident in Figure 4(b)).

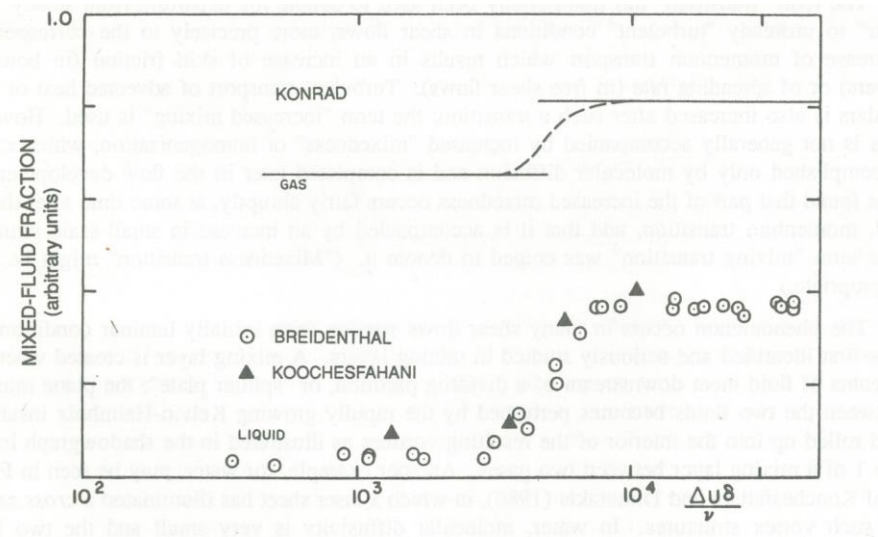

Figure 6 The 'mixing transition' in a free shear layer (Konrad (1977), Breidenthal (1978) Koochesfahani (1984)

Similarly, at higher Reynolds number ($\frac{\Delta U \delta_\omega}{\nu} \approx 10^5$) and also very high Schmidt number (in water) photographs (Dimotakis and Brown (1976)) showed local reactants in the irrotational flow on each side of the mixing layer being entrained by the induced velocity of the large-scale vorticity and then being rapidly mixed to the molecular scale within the large structure.

- **Forcing and control**

The existence of the large scale coherent vorticity suggested ways in which this structure might be influenced or perturbed in order to gain some control over the flow. The experiments of Oster and Wygnanski (1982), for example, in which the trailing edge of a shear layer was oscillated, showed that pure tone forcing could have a substantial effect. The results could be interpreted as a coupling between the forcing and a mode of the turbulent shear layer and as it amplifies it 'wraps up shed vorticity' into clumps of a particular scale and wavelength. These structures, closely similar in strength and spacing, might be described as in a 'meta-stable' state for a period during which the Reynolds stress and growth rate of the mean shear layer are very small, until random disturbances and Biot-Savart interactions again lead to merging and the formation of larger scale structures. Such behavior is easily understood once the underlying coherent structure and mechanics that occurs without forcing, is recognized. Attempts to 'control' turbulent flows (e.g. the base pressure behind bluff bodies or the wall friction through the Thom's effect) are not new but attempts to influence coherent structure to control the flow received a new emphasis.

- **Some Conclusions**
  - Unlike the early emphasis on the mean velocity profile the growth rate of the mixing layer thickness (and the corresponding Reynolds stress) is the key defining parameter.
  - **Stability/Biot-Savart** is the dominant mechanics for the emergence of the large-scale structures in mixing layers and their coalescence to structures of increasing size.
  - There is **chaotic randomness** to the distribution of these structures which leads to a linear growth rate only when many instantaneous realizations are averaged.
  - If Stability/Biot-Savart is the dominant mechanics it should account for the **Reynolds stress** which is then **not local** in an eddy viscosity sense.
  - The thee-dimensionality rides on the large-scale, approximately 2D, structure.
  - **Streamwise vorticity tends to persist** through the coalescence of the large structures. (Reinforced by regions of high strain rate between structures).
  - There is a **mixing transition** at a local Reynolds number of approximately 2×10^3, due to a rapid increase in small scale three-dimensionality, which has at best a weak effect on the Reynolds stress and the growth rate.

- **Some questions**
  - Is there a precise asymptotic growth rate? How much does it differ in two- and three-dimensional shear layers? The asymptotic growth rate as a function of velocity ratio is still not known accurately (better than say 5%), probably because the flow is more sensitive to upstream and downstream boundary conditions than has been fully recognized.
  - Biot-Savart is nonlinear. Is there self-forcing of larger and larger wavelengths? For a 2D inviscid, temporal case what initial conditions are sufficient for the continual coalescence to larger structures?
  - **Is there universality in all turbulent shear flows of a reverse cascade with coalescence of vorticity to larger structures through Biot-Savart?**
  - For a velocity field, which is an integral of the vorticity, how much detail in the vorticity field must be kept to predict the Reynolds stress in free shear flows (which do not have new sources of vorticity at walls or a baroclinic torque)?

4. The plane wake.

Like the mixing layer, other ‘self-preserving’ or ‘equilibrium’ canonical free shear flows have received particular attention with the hope of providing bench-mark data, under well defined conditions, and insight into the basic mechanics of these flows. Since the time of the Marseille meeting various aspects of the plane wake have been clarified but numerous questions remain even for the far wake.

- **The near, mid and far wake and asymptotic wake**

It is useful to think of four basic regions of the Plane Wake and, based on results for a circular cylinder, these are:

Near wake $0 \le x/d \le 4$ (depending on Re). There is a direct interaction between the flow and the cylinder in this region (as is evident, for example, from the measurement of base pressure when a splitter plate is placed in this region and moved toward the base.

Mid wake $4 \le x/d \le 50$. In this region the presence of vortices shed from the cylinder is detectable but changes to this region through a splitter plate, for example, have no direct effect on the flow adjacent to the cylinder.

Far wake $50 \le x/d \le 1000(?)$ In this region there is approximately self-similar behavior of the mean flow. The growth constants, however, are those for the geometry of the body which is the source of the wake even if expressed in terms of the Drag on the body; the downstream limit in the inequality, in particular, is very approximate and variable and is dependent on the source of the wake.

Asymptotic wake $x/d \ge 1000(?)$ The growth constants in terms of the Drag of the body are universal for all two dimensional bodies. Again the lower boundary depends on the source of the wake.

The plane far wake and asymptotic wake distinction

The approximate similarity and growth rate of the far wake and the distinction between the far wake and the asymptotic wake (and the data which supports it) provide a comparison with the mixing layer and raise questions about the development and evolution of the structure in the flow. A summary, based on Townsend (1956) and Narasimha and Prabhu (1972), on which a distinction is made is given in Appendix II.

There remain questions about how rapidly the far wake approaches the asymptotic wake. For example, the results from Wygnanski et al (1986) for wakes from different bodies with more or less intense vortex shedding showed similarity in the velocity profiles and the characteristic dependence of $\overline{u}_0$ and δ on $x - x_0$ as in the far wake (Appendix II), but even where $\overline{u}_0/U_1$ is small ($\overline{u}_0/U_1 = .04$) in some cases the equivalent local value of x_0/x is still approximately 0.25 (assuming they are approaching the asymptotic state).
Behind this issue are basic questions about structure and its potential evolution towards some asymptotic structure which becomes independent of initial conditions. Put simply, the questions of whether there are 'characteristic' large scale structures for an asymptotic plane wake (characterized by the local wake thickness and centerline velocity deficit) and if so, what role do they play, are not settled?

- **Structure in the Plane Wake**

A fundamental difference between the plane wake and the mixing layer is that the wake contains vorticity of <u>both signs</u> "in equal amounts", so to speak. More precisely, the integrals of mean vorticity and mean vorticity flux over the layer are zero:

$$\gamma(x) = d\Gamma / dx = \int_{-\infty}^{\infty} \omega dy = 0 \quad \text{and} \quad \int_{-\infty}^{\infty} U\omega dy = 0 \tag{4.1}$$

A more useful statement is that

$$\frac{d}{dx}\int_{-\infty}^{0} U\omega dy = -\frac{d}{dx}\int_{0}^{\infty} U\omega dy \quad \text{and} \quad \frac{d}{dx}\int_{-\infty}^{0} U\omega dy < 0$$

The fluxes of vorticity above and below the center line $(y = 0)$ are finite but of opposite sign and they are **decreasing** (in absolute value) as the shear layer grows. In either laminar or turbulent wakes, vorticity must be cancelled by opposite signed vorticity that has been transported across $y = 0$, respectively by either molecular diffusion or turbulent transport (as in equation 2.7). In laminar flow the cancellation is by molecular mixing but in turbulent flow large regions of different sign may exist side by side and 'cancellation' occurs in the **averaged** values.

For the mixing layer a single row of one-sign vortices is representative of the basic flow and suggestive of the primary, Kelvin-Helmholtz instability that leads to the structures discussed in the preceding sections. For the wake the corresponding representation is two rows, one of each sign, forming 'vortex streets' with various spacings. In his classic study von Karman found that streets of point vortices are unstable except for the asymmetric (staggered) arrangement at spacing ratio $h/\ell = 0.281$, where it is neutrally stable. The evolution of two sheets approximated by point vortices from a **finite** perturbation was computed by Abernathy and Kronauer in the numerical simulation noted earlier. While two dimensional representations have been quite successful for the mixing layer, there is no assurance that this is the case for the wake. In fact, the double-roller structure inferred by Grant from correlation measurements implies that the primary instability structure is **three dimensional**. But how it might be connected to instantaneous coherent structures passing through the correlation space has been a difficult question. A clue is provided by the instability investigation of Robinson and Saffman (1982) on streets of vortices with finite cores. In addition to the classical perturbation of each row in the two-dimensional plane they added a **span-wise** perturbation to every vortex. They found that, for some combinations of spacing ratio, h/ℓ and span-wise wave length, λ/h, the span-wise amplification rate was comparable to the in-plane rate. The resulting span-wise sinuous structure of each vortex would now have the necessary components of vorticity **normal** to the plane of the wake (plus and

minus) to explain the prominent components in Grant's averaged structure. What actually evolves is not yet quite clear but the pictures of Breidenthal (1980), (Figure 7(a)), and the numerical simulations of Meiburg and Lasheras (1988) indicate that the primary 'coherent' structures are loops which connect the opposite signed vorticity on the opposite sides of the layer. A good discussion is given by Breidenthal. His flow pictures (Figure 7) demonstrate the strong tendency for loop structure to persist in a wake ($U_2 = U_1$, Figure 7(a)), whereas for a mixing layer ($U_2 = 0.4U_1$, Figure 7(b)) the imposed three-dimensional structure gives way to the span-wise-organized vortices. (The seeming two-dimensionality seen in the elevation view in Figure 7(a) conceals the very strong three-dimensionality evident in the plan view, which was generated by the periodic disturbance at the trailing edge.)

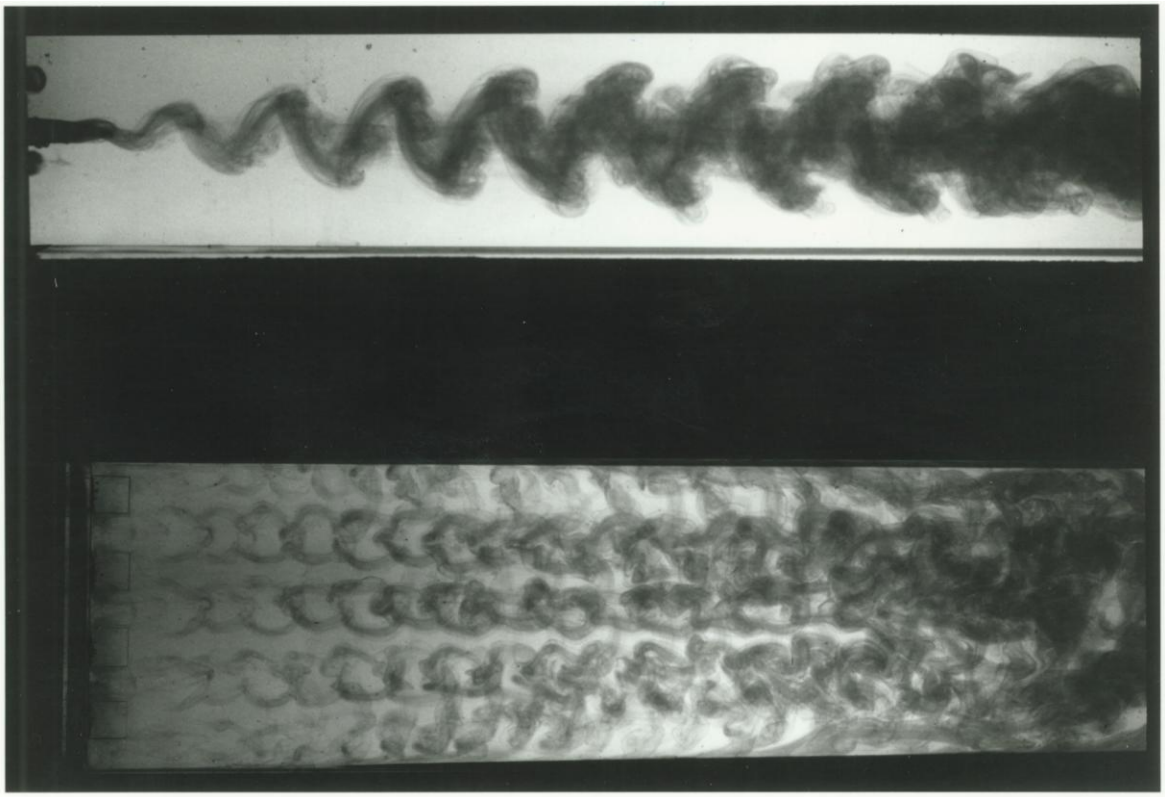

Figure 7(a)

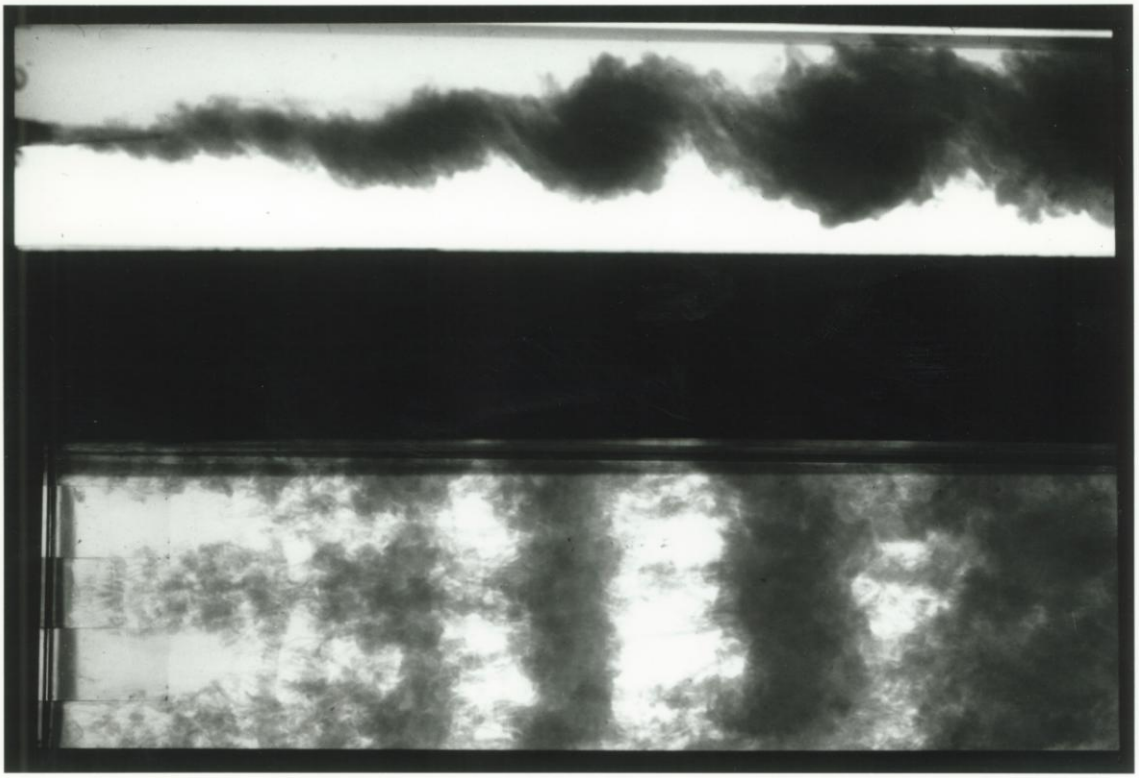

Figure 7(b)

Assuming that 'loop-like' large structure is the primary coherent structure downstream of the near wake, how does it participate in the growth of the wake? Part of it will be due to growth of the loops. This is evident in Breidenthal's photo (Figure 7 (a)) in which the structures are seen to be growing at fixed spacing and not coalescing. Terms in the momentum equation contributing to the growth would include $\overline{v'\omega_z'}$ and $-\overline{w'\omega_y'}$ (see section 2). Such growth would be followed by rescaling of the structure as the increased thickness becomes receptive to instability at lower wave number (larger spacing). The details of this analog of the mixing-layer "merging" process are not yet completely clear but the following gives some useful insights.

Attention to it was first drawn by Taneda (1956) who obtained edge-view visualizations (Figure 8), similar to those in Figure 7(a), of a wake at Re =300 at various locations up to $x/d \simeq 1600$ where it had been rescaled by a factor of approximately 8.5, after several stages (three rescalings would give approximately 2^3). Taneda described the phenomenon as a series of 'rearranged' (we would say **rescaled**) 'Karman vortex streets'. In edge view the asymmetric far-wake pattern looks like the edge of a 'street' because the loops are aligned span-wise. The indication is that the rescaling instability drives the three-dimensional flow toward a particular street spacing (not 0.281) in the

reformed ‘coherent’ structure. ‘Movies’ of the phenomenon are not available, as far as we know, but there are indications that a given stage (2 or higher) will not be replicated in exactly the same x-interval. Thus, as in the mixing layer, it will have a statistical character in any time-series measured at a given value of x.

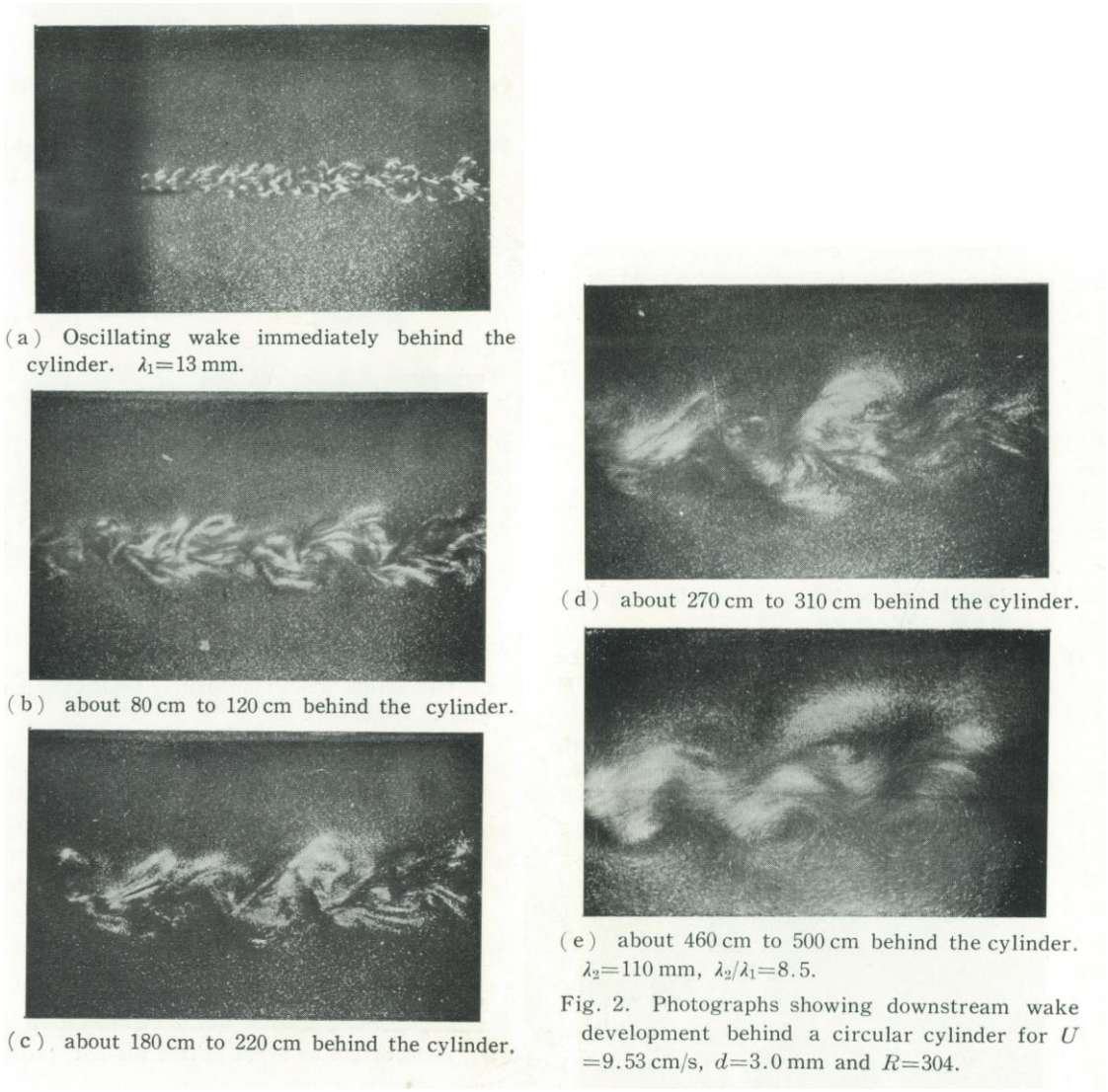

(a) Oscillating wake immediately behind the cylinder. λ_1=13 mm.

(b) about 80 cm to 120 cm behind the cylinder.

(c) about 180 cm to 220 cm behind the cylinder.

(d) about 270 cm to 310 cm behind the cylinder.

(e) about 460 cm to 500 cm behind the cylinder. λ_2=110 mm, λ_2/λ_1=8.5.

Fig. 2. Photographs showing downstream wake development behind a circular cylinder for U =9.53 cm/s, d=3.0 mm and R=304.

Figure 8 Wake rescaling Re=300 (Taneda 1959)

Taneda’s pictures motivated an investigation by Cimbala (1984) at higher Reynolds numbers using smoke-wires for visualization and hot-wire anemometry for mean and fluctuating velocity measurements. Flow patterns similar to Taneda’s were observed at these much higher Reynolds numbers (Figure 9). Additional insight was obtained from experiments on the wake of a porous flat plate, broadside to the flow. With solidity ratio $\sigma = 29\%$ the plate does not shed vortices; smoke lines in the near wake indicate nearly parallel flow (Figure 9(b)). This flow develops a wake instability which, by $x/d = 30$

has grown into a 'street' with a spacing ratio $h/\ell \simeq 1$, considerably larger than the Karman stable value. This is followed by a rescaled stage 2 with spacing ratio $h/\ell \simeq 0.5$.

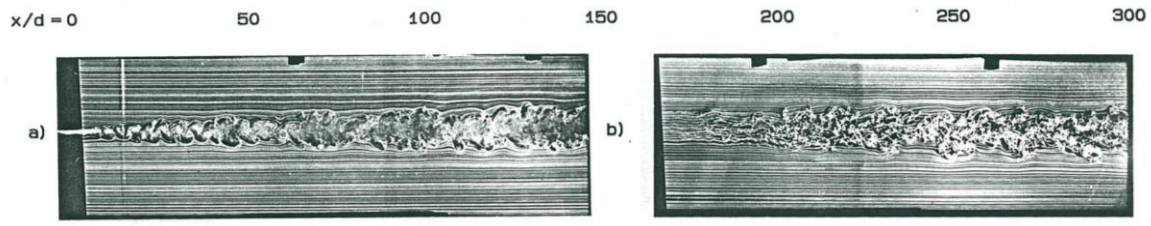

Figure 9(a) Circular cylinder at Re=2200, smoke-wire at (a) $x/d = 1$ and (b) $x/d =$ 180 (Cimbala 1984)

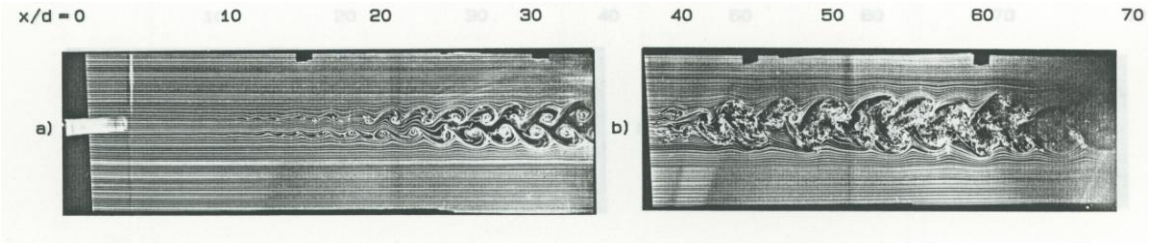

Figure 9(b) Porous flat plate at Re=6800, $\sigma = 29\%$, smoke-wire at (a) $x/d = 0$ and (b) $x/d =$ 38 (Cimbala 1984)

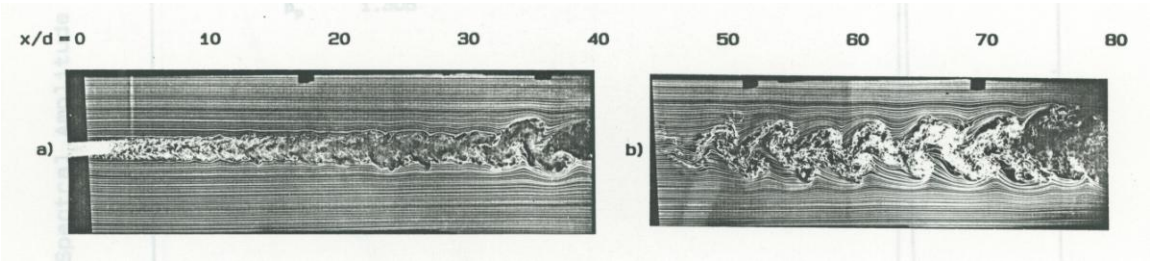

Figure 9 (c) Porous flat plate at Re=6000, $\sigma = 47\%$, smoke-wire at (a) $x/d =$ 0 and (b) $x/d =$ 44 (Cimbala 1984)

Results for a body with higher solidity $(\sigma = 47\%)$, shown in Figure 9 (c), still display no vortex shedding. Small structure in the near wake is followed by organized wake-instability growth and decay, followed by rescaling to stage 2, with $h/\ell \simeq 0.5$. This suggests that rescaling in the wake, like rescaling in the mixing layer, displays the growth and decay of an instability wave at a particular wave number α (i.e. fixed streamwise spacing). With increasing wake thickness $\delta(x)$, the value of $\alpha\delta$ increases and

amplification **rate** $\left(-\alpha_i\right)$ decreases, from an earlier maximum value. When $\left(-\alpha_i\right)$ reaches zero the **amplitude** is at its maximum value, thereafter decaying and setting the stage for rescaling. Some confirmation of such development was obtained from statistical measurements by Cimbala from hot-wire measurements of velocity fluctuation spectra at values of Re up to 500. In particular, maximum amplitude $A(x)$ tended to occur nearer to the neutral (zero) value of $\alpha\delta$ (predicted by linear stability theory for mean wake-profiles) than to the value for maximum amplification rate. This is similar to results from probability distributions of vortex frequency in mixing layers.

The flow pictures from various sources, all at low Reynolds numbers, indicate that the rescaled stages of the 'street' have a spacing ratio $h/\ell \simeq 0.5$. Even at low Reynolds number it is difficult to make a more precise measurement but it was accomplished by Antonia *et al* in the wake of a circular cylinder at $\mathrm{Re} = 1200$ at $x/d = 420$. From digital time series of conditionally measured velocities and temperature-markers, they were able to reconstruct various maps of the velocity field, vorticity, etc. Figure 10 shows the velocity vectors in a coordinate system moving in the x-direction with a suitable convection speed U_C, i.e. one that produces a nearly stationary pattern of centers and saddle points. The spacing ratio $h/\ell = 0.60$. Since $\ell \simeq 15d \simeq 3\ell_1$ we suppose that this is a stage 2 structure, but **not** doubled from stage 1.

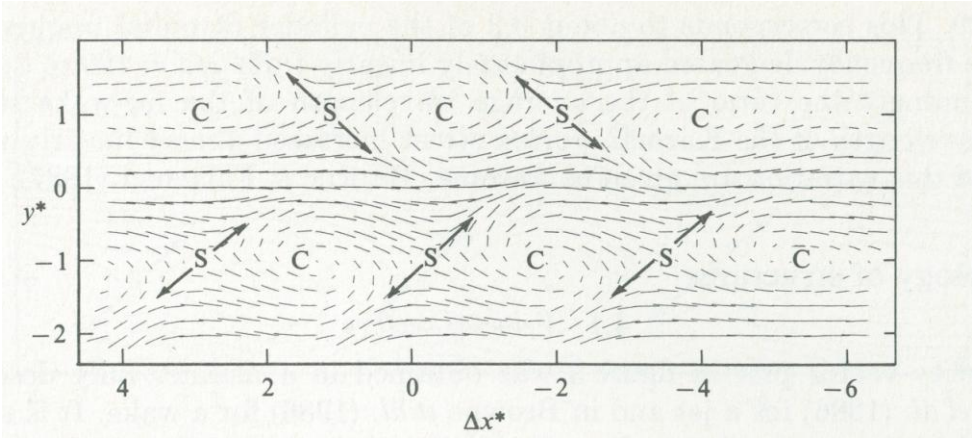

Figure 10 Conditionally-Sampled Velocity vectors in a plane wake at Re=1200 and $x/d = 420$ (Antonia et al)

- **2-D Inviscid Instability and non-linearity**

The results of Abernathy and Kronauer were obtained from a Biot-Savart calculation with two rows of vortices and with 21 vortices per wavelength for the two rows used to approximate the wake. The authors refer to the 'clouds' of vorticity which emerged and Liepmann comments that 'The similarity of the pattern to shadowgraphs of turbulent

wakes is also quite obvious'. With modern computing power a far more realistic representation of the mean velocity profile by rows of vortices of varying strength and fixed spacing is possible. Recently, Suryanarayanan et al (2011) modeled a $\cosh^{-2}\left(y/\delta\right)$ velocity profile with 71 rows each of 78 vortices and the circulation of each vortex chosen to represent the local mean vorticity distribution for this mean velocity profile. This number of vortices per row and arrangement of rows corresponds with a wave-number for the most unstable mode obtained from linear stability theory. The advantage of the Biot-Savart formulation of the inviscid stability problem is that it allows a seamless progression to non-linearity, a straight-forward calculation of the mean Reynolds stress in the linear and non-linear regimes (as described in Section 2) and an opportunity to see a possible rescaling to longer wavelength instability. By 'experimentally' varying the initial spacing of the vortices in each row to match a vorticity Eigen mode which develops (grows exponentially), exponential growth is obtained from $t=0$ for a very small initial displacement amplitude. The result of this initial growth is an exponentially growing mode which has almost exactly the theoretical growth rate. To explore the non-linear development the domain was then doubled in the x direction and the number of vortices reduced by half and their strength doubled. The results for increasing non-dimensional time are shown in Figure 11. The way in which the vorticity 'clumps' and the velocity field becomes dominated by this concentration of vorticity is very evident. Entrainment occurs evidently by the engulfment of fluid due to the large scale vorticity and a 'nibbling' of an active 'superlayer' is not at all representative of the mechanics in this two dimensional case.

$t=0$

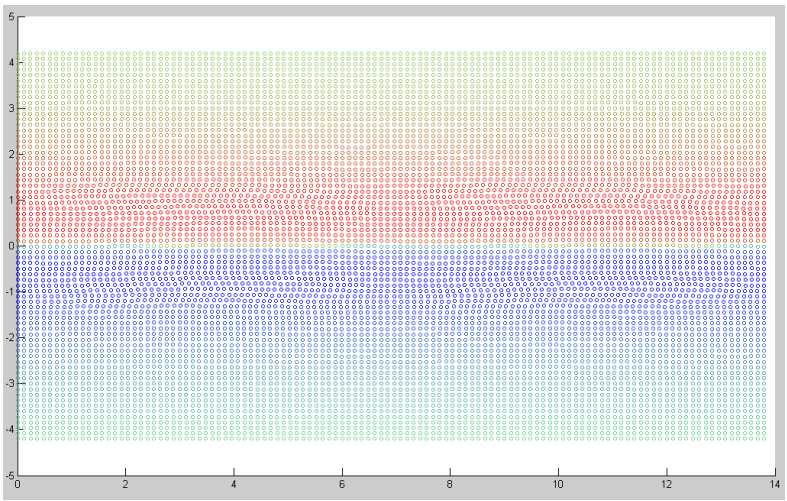

$t = 20$

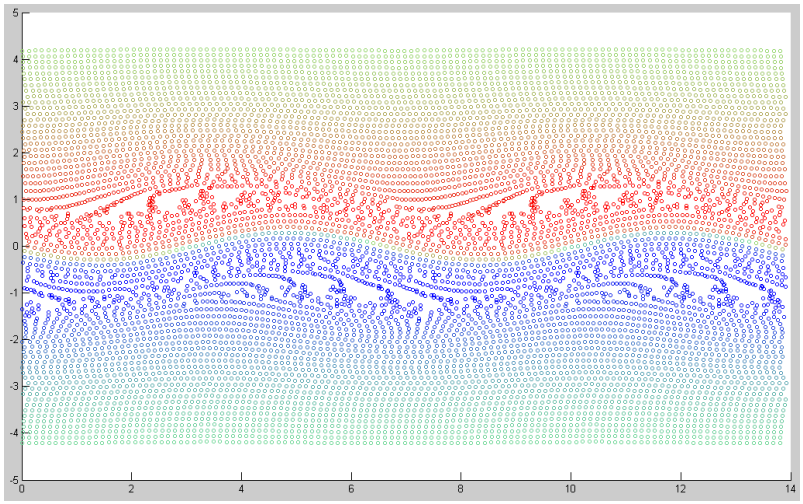

$t = 40$

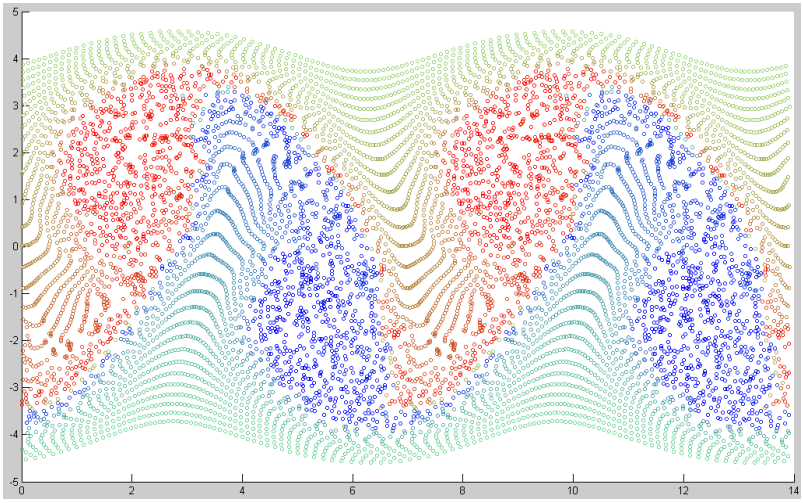

$t = 60$

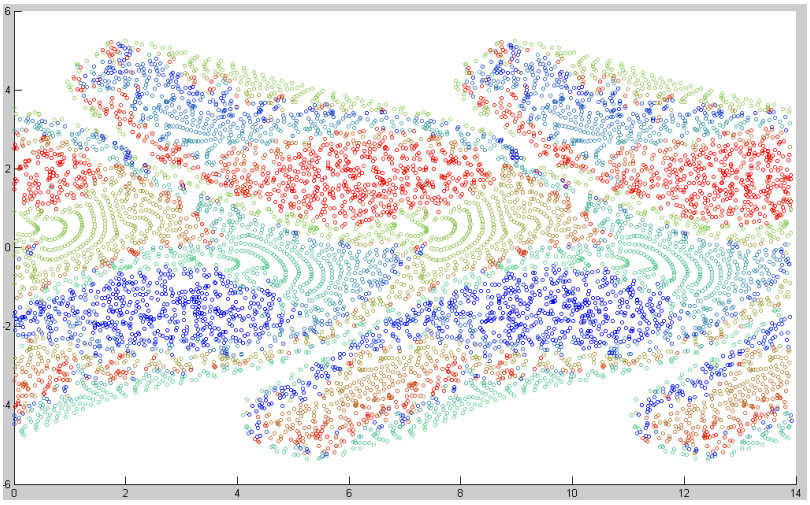

$t = 120$

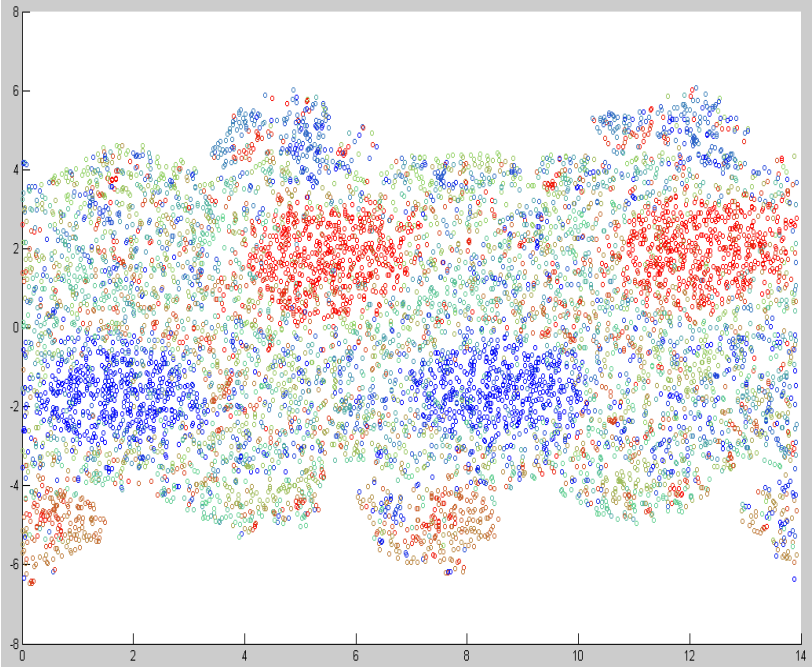

$t = 170$

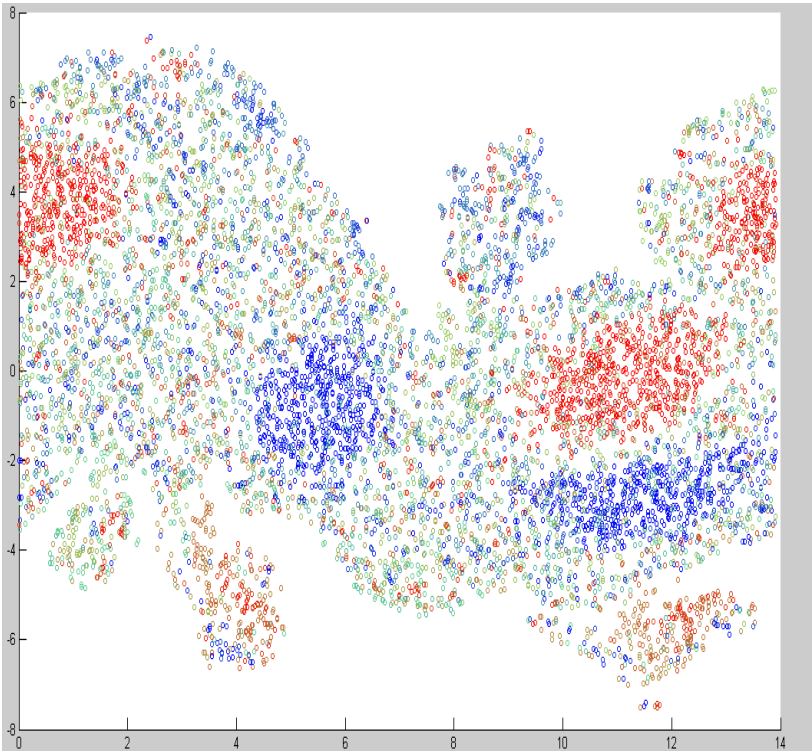

Figure 11, A point vortex simulation of a 2D wake instability, t=0,20,40,60,120,170 (Suryanarayanan et al (2011)

The initial modal growth shows a peak Reynolds stress near the time at which the amplitude of the fundamental is a maximum. There is then a subsequent decay of this mode, the transport of vorticity of opposite sign across the layer, followed by growth in the mean velocity profile and the emergence of larger wavelength instability even though it was initially **not** directly imposed. As with the results 50 years ago what is interesting is the non-linear evolution of this 'simple' 2-D flow and the extent to which it may illuminate an underlying tendency for vorticity to clump to large scales through Biot-Savart creating a velocity field that 'accounts for' the vorticity transport and the entrainment of irrotational fluid.

- **Vorticity flux in the plane wake.**

There is a wide range of experimental measurements of the near wake of a circular cylinder at Re=10,000 but a detailed resolution of the vorticity field and the measurement of vorticity fluxes has not been possible. That this Reynolds number is now accessible, with a limited span-wise domain of approximately three diameters, to an LES calculation (Mani, Moin and Wang 2009) provides a new opportunity to explore directly aspects of the vorticity transport. The LES results give a Strouhal number of 0.193 and a base pressure coefficient of -1.35 which should be compared with the experimental values of 0.20 and -1.15, respectively. The base pressure is still somewhat sensitive to shear layer transition at this Reynolds number but there remain questions about the discrepancy in base pressure and the absolute accuracy of such a calculation. Nevertheless, it provides a special opportunity to 'see' the vorticity field, the role of various instabilities, the behavior of the vorticity flux, and the 'initial conditions' from which the far wake develops. The database from the calculation has been provided by Ari Mani and Parviz Moin. (Mark Lohry has worked with one of us (GLB) to manipulate it.) Figures 12 (a) and (b) show respectively an instantaneous picture at the same time of the span-wise vorticity and the span-wise averaged vorticity (averaged over the full span πD of the calculation). What is striking is how much of the shed vorticity is widely distributed into the near wake as a result of the Kelvin-Helmholtz instability in the separating shear layers, the three-dimensionality of this shed vorticity and the large scale velocity field imposed by the shed vortices. The result is a large flux of vorticity, as given by equation (2.7), across $y = 0$ in the near wake.

The contributions to this mean flux, as functions of x/D, are shown in Figure 13 (a), (where the averages were taken over only two periods). Interestingly, the **largest** component is $\overline{V\Omega}$ where $V(x, y, t)$ is the span-wise averaged normal component of the velocity and $\Omega(x, y, t)$ is the span-wise averaged, span-wise vorticity. The global character of the corresponding Reynolds stress field is clear. As discussed in section 2,

since the source of vorticity on the upper half of the cylinder is equal to the net flux out of a control volume (formed by the plane $y = 0$ from the base and the plane $x = X$) then the integration of the vorticity flux from the base to $x = X$ on $y = 0$ (as in equation 2.7) will show how much of the shed vorticity has been 'lost' or 'cancelled' (the remainder being a flux across the plane $x = X$) . Since the mean flux of vorticity supplied at the wall is approximately 0.047 for this calculation, Figure 13 (b) shows that one half of the vorticity supplied at the wall is cancelled within one diameter from the base.
Importantly this flux across $y = 0$ is also directly connected to the base pressure. An alternative form of equation (2.5) may be obtained from a line integral of the momentum equation about a fixed contour. That is

$$\frac{\partial \boldsymbol{u}}{\partial t} + \nabla\left(\frac{1}{2}\boldsymbol{u}\cdot\boldsymbol{u}\right) + \boldsymbol{\omega}\times\boldsymbol{u} = -\frac{1}{\rho}\nabla p + \nu\nabla^2\boldsymbol{u}, \tag{4.2}$$

so that

$$\frac{d}{dt}\oint \boldsymbol{u}\cdot d\boldsymbol{r} + \oint \boldsymbol{\omega}\times\boldsymbol{u}\cdot d\boldsymbol{r} = -\nu\oint \nabla\times\boldsymbol{\omega}\cdot d\boldsymbol{r} \ , \tag{4.3}$$

where the identity $\nabla\times(\nabla\times\boldsymbol{u}) = \nabla(\nabla\cdot\boldsymbol{u}) - \nabla^2\boldsymbol{u}$ is used. The contribution to a line integral of equation (4.2) between two fixed points gives, for a steady high Reynolds number free turbulent flow in which the mean viscous stresses can be neglected,

$$\nabla\left(\frac{\overline{p}}{\rho} + \frac{1}{2}\boldsymbol{U}\cdot\boldsymbol{U} + \frac{1}{2}\overline{\boldsymbol{u}'\cdot\boldsymbol{u}'}\right)\cdot d\boldsymbol{r} = \Delta\left(\frac{\overline{p}_T}{\rho}\right) = \left(\boldsymbol{U}\times\boldsymbol{\Omega} + \overline{\boldsymbol{u}'\times\boldsymbol{\omega}'}\right)\cdot d\boldsymbol{r} \tag{4.4}$$

Thus

$$\frac{\overline{p}_T(X)}{\rho} - \frac{\overline{p}_B}{\rho} = \int_{D/2}^{X}\left(\overline{v'\omega_z'} - \overline{w'\omega_y'}\right)dx \tag{4.5}$$

The left-hand side and right-hand side of equation (4.5) have been plotted in Figure 13 (b). From the figure, by $x/D = 9.6$ the non-dimensional flux is approximately .036 and the remaining flux is approximately .011 (total approx .047). Of course these LES calculations include a Smagorinsky diffusion and this contribution has not been included. Nevertheless, such calculations offer new possibilities in understanding the mechanics of the vorticity, which generates through Biot-Savart the velocity field and which in turn gives rise to the vorticity transport and the transport of momentum in high Reynolds number free turbulent shear flows.

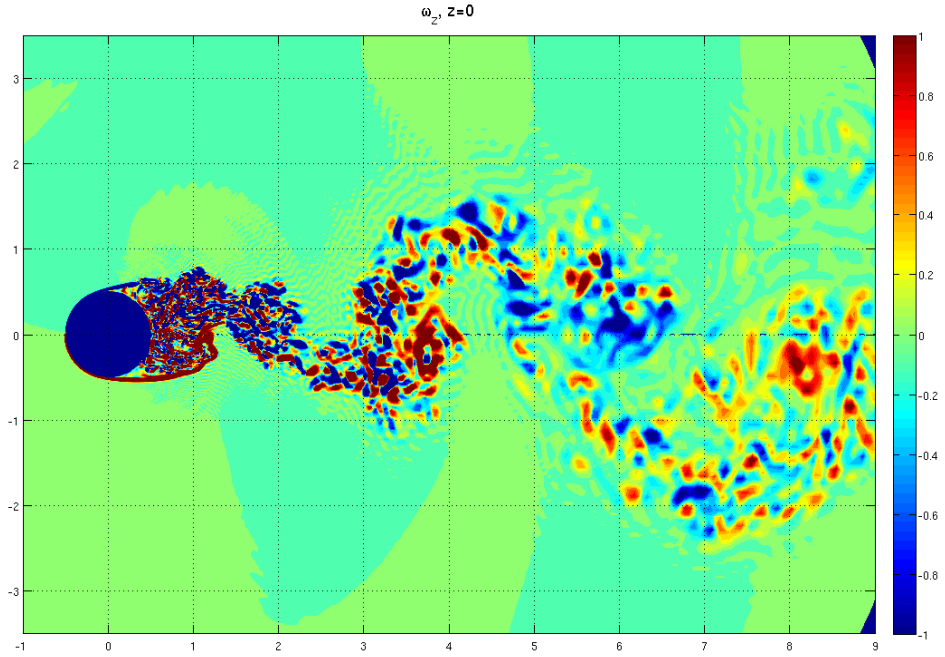

Figure 12 (a) Distribution of span-wise vorticity at a particular time on $z/D = 0$ from an LES calculation (Mani et al (2009))

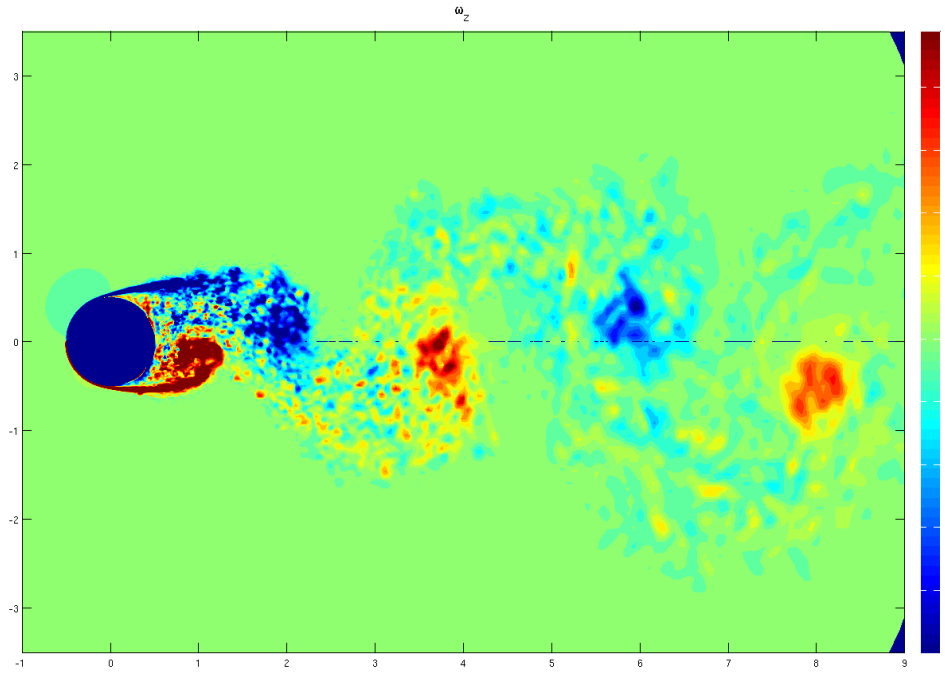

Figure 12 (b) Span-wise averaged distribution of span-wise vorticity at a particular time from an LES calculation (Mani et al (2009)

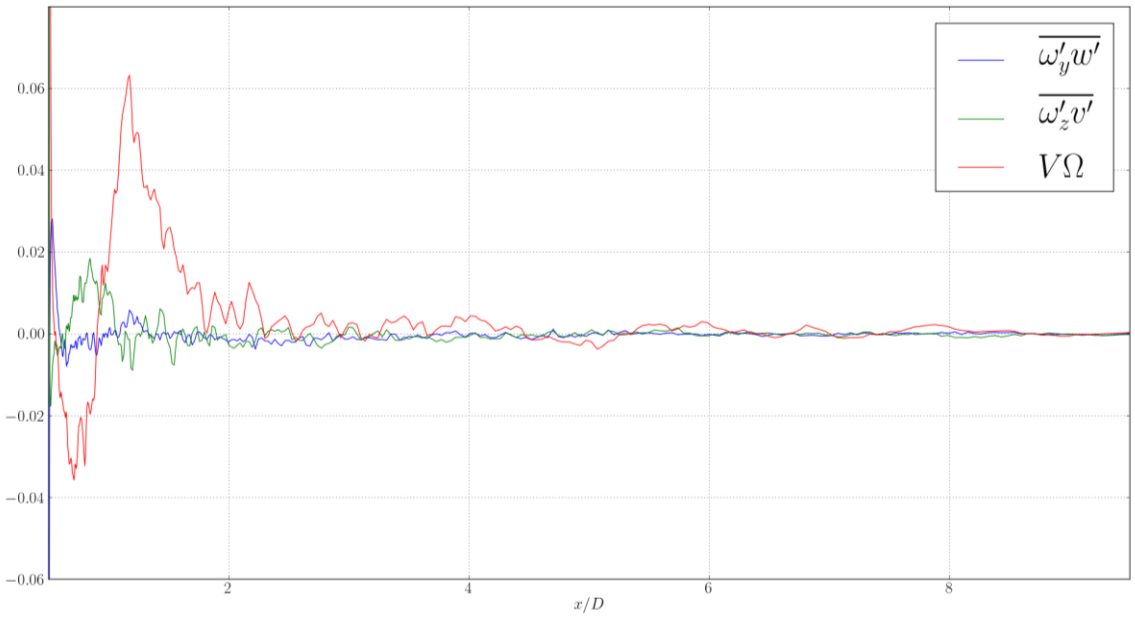

Figure 13 (a) Three components of the mean vorticity flux on $y = 0$

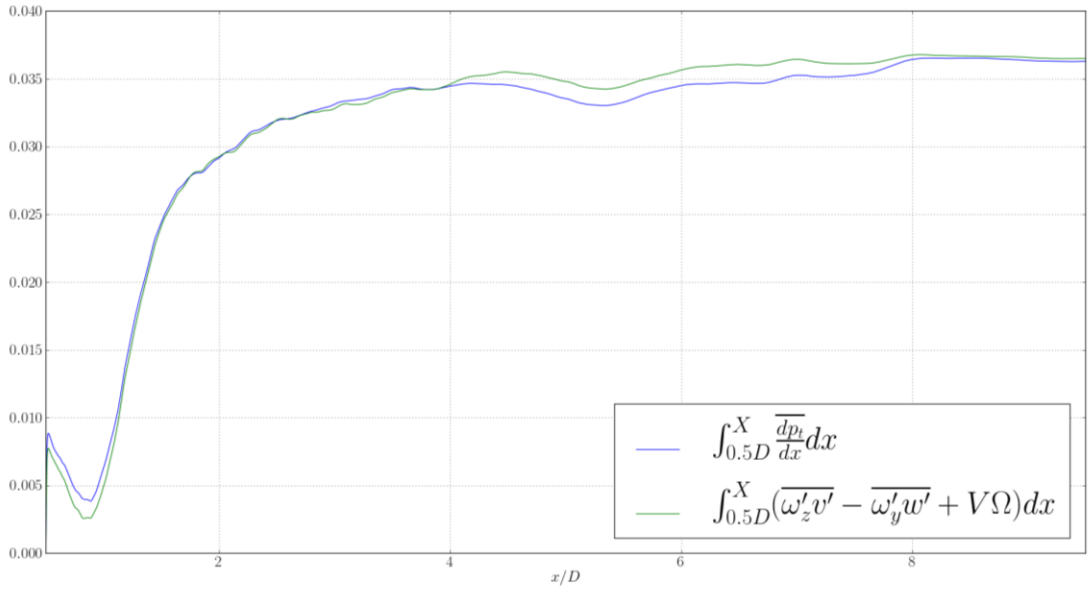

Figure 13 (b) The integral of the vorticity flux on $y = 0$ and the integral of the total pressure.

- **Some Conclusions**

  - Even though the turbulent wake is a highly three-dimensional flow there is considerable evidence that there is rescaling of a vortex-street like structure which is characterized by groups of 'span-wise vorticity' localized in the streamwise and span-wise directions with values for h/ℓ nearer to 0.5-0.6 than the classical, neutrally stable value for point vortices of 0.281.
  - In particular the conditional sampling which led to the velocity field obtained by Antonia et al at a Reynolds number of 1200 and $x/d = 420$ shows a remarkable degree of organization over several stream-wise wavelengths. These results give a wavelength 2-3 times larger than that of the vortex street formed in the near wake and provide strong evidence of an underlying rescaling mechanism. The experimental results by Cimbala at even higher Re show this rescaling and they are consistent with a view that the basic clumping of the vorticity has its origin in instability/Biot-Savart.
  - The three-dimensional instability found at low Reynolds number and supported by various theoretical and computational studies appears to manifest itself in the form of vortex loops connecting the primary upper and lower span-wise vorticity.
  - Much of the span-wise vorticity shed into the near wake is strongly affected by local instabilities in the shear layer and the large scale velocity field imposed by Biot-Savart from the accumulation of this vorticity in the shed vortices. In particular the large net flux across the $y = 0$ plane in the immediate near wake substantially reduces the circulation of the shed vortices and also provides a different insight into the base pressure and near-wake structure.

- **Some questions**
  - Does the structure rescaling continue for wakes at much higher Reynolds numbers?
  - Is there an asymptotic, high Reynolds number wake characterized only by the drag of the body (momentum thickness) and the distance from the body. This implies a universal structure which seems likely to require a large number of re-scalings from the first-formed vortex street.
  - How much does the growth rate of a two-dimensional wake differ from the three-dimensional one?

5. Concluding Remarks.

- At the time of the Marseille meeting in 1961 a goal for free turbulent shear flows was to find a constitutive relation for the turbulent or 'turbular' fluid and to take into account the relatively sharp interface (at high Reynolds numbers) between the irrotational and rotational fluid. In some respects it was an extension of an earlier goal to seek an eddy viscosity formulation that would enable the mean velocity profile to be predicted.

- In the last 50 years considerable progress has been made in illuminating the mechanics of the mixing layer. There is now recognition of the central role played by instability and the Biot-Savart relationship which leads to the merging of the one-sided vorticity to form organized clumps of increasing scale. The 'mixing transition' that was found accounts for the rapid mixing to molecular scales in a high Reynolds number mixing layer. Similarly the presence of the 'coherent structure' and an appreciation of the underlying mechanics has accounted for the response at some frequencies to external forcing and also for the dependence of entrainment ratio of the two free streams on their density ratio (though we have not discussed it here).

- Much less is known about the underlying coherent structure in the plane wake and other free shear flows in which the mean vorticity distribution is not one-sided. The experimental and numerical results presented and results for other free shear flows suggest that the vorticity field also tends to form organized clumps, basically through the well-known mechanics of linear instability or more generally (i.e. including non-linearity) through the Biot-Savart interaction. Results at relatively low Reynolds number suggest that the coherent structure in plane wakes, although three-dimensional, is organized by span-wise vorticity, as in mixing layers.

- An understanding of the mechanics is most likely to be obtained from the vorticity field. *The subject stands at the beginning of a new era in which both LES and DNS calculations can provide details of the vorticity field and the fluxes of vorticity (vortex force).* In this respect there is a new opportunity to treat numerical computations much like experiments and to use them to seek not only simulations but an understanding of the essential mechanics.

- Figure 14 is a photograph of the last launch of the Shuttle. The Reynolds number of the far-field co-flowing jet is estimated to be of the order of $10^9 - 10^{10}$. An underlying 'coherent structure' resulting from the clumping of the vorticity seems self evident. Will LES predict it and show the underlying mechanics and momentum transport? That could be a challenge that might be met in Marseille in 2061.

Figure 14. The last launch of the Shuttle, July 8th 2011

References:

APPENDIX I

Reynolds stress and the Vorticity flux

The familiar vector identity (for $\nabla \cdot \boldsymbol{u} = 0$)

$$\boldsymbol{u} \cdot \nabla \boldsymbol{u} = \boldsymbol{\omega} \times \boldsymbol{u} + \nabla(\frac{1}{2}\boldsymbol{u} \cdot \boldsymbol{u}), \tag{6}$$

written in summation notation, using $\frac{\partial u_k}{\partial x_k} = 0$, is

$$\frac{\partial u_i u_k}{\partial x_k} = \varepsilon_{ijk}\omega_j u_k + \frac{\partial}{\partial x_i}(\frac{1}{2}u_k^2) \tag{7}$$

Since $\nabla \cdot \boldsymbol{u} = 0$ for the instantaneous as well as the mean velocity, and therefore also for the fluctuating components of the velocity, the identity (2) applies also to the fluctuating components of the velocity u_i' and it follows that

$$\frac{\partial u_i' u_k'}{\partial x_k} = \varepsilon_{ijk}\omega_j' u_k' + \frac{\partial}{\partial x_i}(\frac{1}{2}u_k'^2) \tag{8}$$

When equation (3) is averaged over time the gradient of the Reynolds stresses may be written in terms of the mean correlation in the vorticity and velocity fluctuations together with the gradient of the mean turbulence kinetic energy.

APPENDIX II

The Plane Far Wake and the Asymptotic Wake

For the plane wake, if the mean velocity defect is $\bar{u}(x,y) = U_1 - U(x,y)$ then, if the normal Reynolds stresses, which give small departures in the static pressure and streamwise momentum flux, are neglected the drag is

$$Drag = \rho \int_{-\infty}^{+\infty} U(U_1 - U)\, dy = \rho \int (U_1 - \bar{u})\bar{u} dy \equiv \rho U_1^2 \theta, \tag{9}$$

where θ is the momentum thickness of the wake. For a body of characteristic dimension D and a the drag coefficient C_D, θ/D is $\frac{1}{2}C_D$. Thus to this approximation momentum conservation requires that the length θ is independent of x for a body with a given drag.

If, at high Reynolds number, the effect of viscosity on the mean flow in the wake can be ignored and if $\bar{u}_0$ is the mean velocity deficit on the centerline and δ is the half width of the wake (where the mean velocity is $\frac{1}{2}\bar{u}_0$) dimensional analysis gives (for a 2-D body defined by n dimensions, D_n),

$$\frac{\bar{u}(x,y)}{U_1} = f_1\left(\frac{x}{\theta},\frac{y}{\theta},\frac{D_n}{\theta}\right) \text{ and } \frac{-\overline{u'v'}(x,y)}{U_1^2} = f_2\left(\frac{x}{\theta},\frac{y}{\theta},\frac{D_n}{\theta}\right)$$

so that $$\frac{\bar{u}_0}{U_1} = f_3\left(\frac{x}{\theta},\frac{D_n}{\theta}\right) \quad \text{and} \quad \frac{\delta}{\theta} = f_4\left(\frac{x}{\theta},\frac{D_n}{\theta}\right),$$

and therefore $$\frac{\bar{u}(x,y)}{\bar{u}_0} = f_5\left(\frac{y}{\delta},\frac{\theta}{x},\frac{D_n}{\theta}\right) \text{ and } \frac{-\overline{u'v'}(x,y)}{\bar{u}_0^2} = f_6\left(\frac{y}{\delta(x)},\frac{\theta}{x},\frac{D_n}{\theta}\right) \tag{10}$$

If $\theta/x \to 0$, the wake defect $\bar{u}$ exhibits similarity for a given body since $\frac{\bar{u}(x,y)}{\bar{u}_0(x)} = f_5\left(\frac{y}{\delta(x)},0,\frac{D_n}{\theta}\right)$ and it has been well established (Townsend 1956, Uberoi and Freymuth 1969, Symes and Fink 1977, Yamada 1980) that for the far wake the shape of the velocity profiles becomes independent of D_n/θ so that

$$\frac{\bar{u}(x,y)}{\bar{u}_0(x)} = f_7\left(\frac{y}{\delta(x)}\right) \tag{11}$$

This equation for $\bar{u}$ applied now in the conservation of momentum equation (4) leads to the expression

$$\frac{\theta}{I_1\delta} = \frac{\bar{u}_0}{U_1}\left(1-\frac{I_2}{I_1}\frac{\bar{u}_0}{U_1}\right), \tag{12}$$

where, following Townsend, $I_1 = \int_{-\infty}^{\infty} f_7\left(\frac{y}{\delta}\right)d\left(\frac{y}{\delta}\right)$ and $I_2 = \int_{-\infty}^{\infty} f_7^2\left(\frac{y}{\delta}\right)d\left(\frac{y}{\delta}\right)$. The first term corresponds with the neglect of terms (including the anticipated normal Reynolds stress terms) in equation (4) of order $\bar{u}_0^2/U_1^2$ compared with $\bar{u}_0/U_1$. (Thus, for the far wake, where $\bar{u}_0/U_1$ is small, the product $\bar{u}_0\delta \to const$ since $\frac{U_1\theta}{\bar{u}_0\delta} = I_1 - I_2\frac{\bar{u}_0}{U_1}$)

Similarly for $\theta/x \to 0$ the Reynolds stress from equation (5) will exhibit similarity for a given body. In addition to satisfying the continuity equation, similarity expressed by equation (6), requires the reduction of the momentum equation to an ordinary differential equation in which the coefficients are independent of x. If $\bar{u}_0/U_1 \to 0$ and all viscous and

normal stresses are neglected, the x momentum equation is approximated by $-U_1 \frac{\partial \bar{u}}{\partial x} = \frac{\partial(-u'v')}{\partial y}$. It then follows that to this lowest order the Reynolds stress $-u'v'$ from equation (5) must exhibit similarity

$$-u'v'(x,y) = \bar{u}_0^2 f_8\left(\frac{y}{\delta(x)}\right),$$

and the x momentum equation reduces to

$$-\left[U_1 \frac{\bar{u}_0 \delta}{\bar{u}_0^3} \frac{d\bar{u}_0}{dx}\right] \frac{d}{d\eta}(\eta f_7) = f_8', \tag{13}$$

since to this approximation, from equation (7) $\bar{u}_0 \delta = U_1 \theta / I_1$. Similarity requires the term in the square brackets to be constant and if it is put equal to k then

$$\tfrac{1}{2} \frac{d}{dx}\left(\frac{U_1^2}{\bar{u}_0^2}\right) = \frac{kI_1}{\theta}. \tag{14}$$

Integration gives an asymptotic solution for $\bar{u}_0 / U_1 \to 0$,

$$\frac{\bar{u}_0^2 x}{U_1^2 \theta} = \frac{1}{2kI_1} \tag{15}$$

and from equation (7)

$$\frac{\delta^2}{\theta x} = \frac{2k}{I_1} \tag{16}$$

In the experiments of Narasimha and Prahbu (1972) and further by Sreenivassan and Narasimha (1982) they found $I_1 = 2.05$, $\frac{\delta^2}{\theta x} = .089$ and $\frac{\bar{u}_0^2 x}{U_1^2 \theta} = 2.54$.

If the higher order terms are kept in the momentum integral, as in equation (7), and also the higher order terms in the x momentum equation (i.e. the same order as $V \frac{\partial U}{\partial y}$) and similarity arguments made for the coefficients to be independent of x then Townsend (1956) and Narasimha and Prabhu (1972) found that equations (10) and (11) give respectively the leading term in asymptotic expansions and that

$$\frac{\bar{u}_0^2 x}{U_1^2 \theta} = \frac{1}{2kI}\left(1 + O\left(\frac{\theta}{x}\right)^{\frac{1}{2}}\right) \tag{17}$$

$$\frac{\delta^2}{\theta x} = \frac{2k}{I}\left(1 + O\left(\frac{\theta}{x}\right)^{\frac{1}{2}}\right), \tag{18}$$

as $\theta/x \to 0$. For finite θ/x equations (12) and (13) could be separately approximated by $\frac{\bar{u}_0}{U_1} \propto \left(\frac{(x-x_0)}{\theta}\right)^{-\frac{1}{2}}$ and $\frac{\delta}{\theta} \propto \left(\frac{(x-x_0)}{\theta}\right)^{\frac{1}{2}}$ over some range of θ/x. As is widely accepted we identify the far wake as one for which $\theta/x \ll 1$ and, correspondingly, $\frac{\bar{u}_0}{U_1} \propto \left(\frac{(x-x_0)}{\theta}\right)^{-\frac{1}{2}}$ and $\frac{\delta}{\theta} \propto \left(\frac{(x-x_0)}{\theta}\right)^{\frac{1}{2}}$ and define the asymptotic wake as the region where $x_0/x \to 0$ and for which equations (10) and (11) would apply.